Running title: *in vitro* β-glycan synthases synthase activity

Author for correspondence:
Dr. Ahmed Faik
Department of Environmental and Plant Biology
Ohio University
Athens, OH 45701
Tel.: (740)-593-1130; Fax: (740)-593-1130

Title: New insights on β-glycan synthases using *in vitro* GT-array (*i*-GT-ray) platform

Authors: Matrika Bhattarai[1,2], Qi Wang[3], Hao Chen[3], and Ahmed Faik[1,2]

Affiliations: [1]From the Department of Environmental and Plant Biology, [2]Molecular and Cellular Biology program, Ohio University, Athens, OH 45701, [3]The Department of Chemistry & Environmental Science, New Jersey Institute of Technology, Newark, NJ, 07102

CRediT authorship contribution

M.B., Q.W., H.C., and A.F. designed the research; M.B., and Q.W. performed the research, M.B., Q.W., H.C., and A.F. analyzed the data, and A.F wrote the paper with the help from the other co-authors.

Funding information:

This work was funded primarily by the USDA (Award number 2019-67030-29670) and Ohio University Research Committee (OURC) to AF. HC also thanks support from NSF (Award number CHE-2203284).

Author for correspondence: Ahmed Faik (faik@ohio.edu)

Key words: Glycosyltransferase, plant cell wall, biosynthesis, β-glycan, hemicellulose, NAPPA

This article contains supporting information.

Declaration of competing interest

The authors declare that they have no conflicts of interest with the contents of this article.

Data availability

Data will be made available on request.

Abstract

Cellulose and hemicellulose are the major structural β-glycan polysaccharides in cell walls of land plants. They are characterized by a backbone of β-(1,3)- and/or β-(1,4)-linked sugars such as glucose, mannose, or xylose. The backbones of these polymers are produced by processive glycosyltransferases (GTs) called synthases having multiple transmembrane domains anchoring them to the membrane. Thus, they are among the most difficult membrane proteins to test *in vitro* and to purify. Previously, we developed an *in vitro* GT-array (*i*-GTray) platform and showed that non-processive type II membrane GTs could be produced in a soluble and active form in this platform *via* cell-free system. To determine whether *i*-GT-ray platform is adequate for the production and testing of plant cell wall synthases, we tested five synthases involved in cellulose, xyloglucan, (gluco)mannan, and β-(1,3)(1,4)-mixed-linkage glucan synthesis. Our results revealed unsuspected features of these enzymes. For example, all these synthases could be produced in a soluble and active form in the absence of detergent, membrane lipids, or accessory proteins and none of them required a primer for initiation of synthesis. All synthases produced ethanol-insoluble products that were susceptible to the appropriate hydrolases (i.e., cellulase, lichenase, mannanase). Using this platform, we showed that *At*CslC4 and *At*XXT1 interact directly to form an active xyloglucan synthase complex that produced xylosylated cello-oligosaccharides (up to three xylosyl residues) when supplied with UDP-Glc and UDP-Xyl. *i*-GTray platform represents a simple and powerful functional genomics tool for discovery of new insights of synthase activities and can be adapted to other enzymes.

1. Introduction

The plant extracellular matrix (ECM) forms a cell wall that is dynamic and plays an essential role in plant development and holds great promise as raw material for biofuel production, food, and health products (Ferguson, 1999; Dhugga, 2007; Faik, 2010). Plant cell walls consist primarily of a network of cellulose microfibrils that are cross-linked by glycan polymers and surrounded by a matrix of pectin polysaccharides. Diverse types of cross-linking β-glycans are known and all have in common a linear β-(1,4) and/or (1,3)-linked backbone composed of one type of monosaccharide (glucose, xylose, or mannose) bearing (or not) short side chains of other monosaccharides, such as galactose, xylose, arabinose, and fucose. Both the backbone and the side chains of these glycans vary depending on the species, tissues, and developmental stages. While the major hemicellulose in the primary cell walls of dicots is xyloglucan (XyG, which consists of β-(1,4)-linked glucosyl residues), heteroxylans (HXs, which consist of β-(1,4)-linked xylosyl residues) are the main hemicellulose in primary and secondary cell walls of monocots.

These glycans are the products of specialized enzymes called glycosyltransferases (GTs), which often work in a concerted manner as multi-GT synthase complexes (Taylor et al., 2003; Atmodjo et al., 2011; Chou et al., 2015; Jiang, et al., 2016; Zeng et al., 2016; Amos and Mohnen, 2019). The best characterized of these complexes are cellulose synthase complexes (CSCs), which have a central GT core consisting of at least three non-redundant cellulose synthase (CesA) isoforms, as well as other non-GT proteins (Taylor et al., 2003; Morgan, et al., 2013; Slabaugh, et al., 2014; Endler, et al., 2015). Expression of CesA8 isoforms from *Populus tremula x tremuloides* (*Ptt*CesA8) in *Pichia pastoris* and the reconstitution of purified *Ptt*CesA8 into proteoliposomes demonstrated that a single isoform is sufficient to form cellulose fibers (Purushotham, et al., 2016). However, the catalytic activity required the presence of a lipid bilayer environment and divalent manganese cations. In contrast to CSCs, the composition and assembly of synthases for other β-glycans (i.e., XyG, HXs, mannan, etc.) are less characterized. For example, the *in vitro* synthesis of XyG by microsomal membranes has been extensively studied and was shown to involve coordinated mechanism between XyG β-(1,4)-glucan synthase (XyG-GS) and XyG xylosyltransferase (XXT) activities, in which both UDP-glucose (UDP-Glc) and UDP-xylose (UDP-Xyl) must be supplied for XyG synthesis to proceed (Gordon and Maclachlan, 1989, Hayashi, 1989; Faik et al., 2002). Five Arabidopsis XXT enzymes, *At*XXT1-5 (GT34 family) (Faik et al., 2002; Cavalier, et al., 2008; Zabotina, et al., 2008) and potentially five Arabidopsis

XyG-GS from cellulose synthase-like C (CslC) subfamily (GT2 family) have been identified (Kim, et al., 2020). More recently, the structures of *At*XXT1 have been resolved without ligands and in complexes with UDP and cellohexaose (C_6) (Culbertson, et al., 2018). However, despite this progress, efforts to isolate or reconstitute *in vitro* an active XyG synthase complex have failed and the specific roles of each XXTs in XyG synthase complex remain unclear. Solubilization of the XyG synthase activity from microsomal membranes has always resulted in inactivation of the activity (Hayashi, 1989). In the case of heteroxylans, the biochemical mechanism of β-(1,4)-xylan backbone is far from understood. Recently, we showed the presence of several xylan synthase complexes (XSCs) in rice having central cores made up of various combinations of members of the GT43 and GT47 families (Javaid, et al., 2024). While cellulose, XyG, and heteroxylans appear to be synthesized by multi-GT synthase complexes, both mannan (Liepman, et al., 2005; Voiniciuc, et al.,2019) and mixed-linkage β-(1→3)(1→4)-D-glucan (MLG) (Burton, et al., 2006; Doblin, et al., 2009) appear to be synthesized by single GTs (*i.e.,* CslA9 and CslF6, CslH1, respectively). However, it can't be ruled out whether their activity is modulated by homodimer/multimer complexes.

The fact that GTs are integral membrane proteins present in extremely low amounts in cells makes them among the most difficult proteins to purify and to test *in vitro* (Welner, et al., 2017). Thus, only a limited number of plant cell wall polysaccharide synthases have been tested *in vitro*. In this work, we show that a recently developed *in vitro* GT-array (*i*-GT-ray) screening platform for non-processive GTs based on cell-free coupled *in vitro* transcription/translation (Wang, et al., 2020; Bhattarai et al., 2024; Javaid, et al., 2024), can be adapted for testing of polysaccharide synthases *in vitro* and gain new insights about the biochemical mechanism of the biosynthetic process. Using this platform, we show that: *i*) β-glycan synthases for synthesis of cellulose (*At*CesA4), (gluco)mannan (*At*CslA9), XyG (*At*CslC4), and MLG (*Hv*CslF6 and *Hv*CslH1), can be produced through cell free IVTT systems in a soluble and active form in absence of detergent, membrane lipids, or any accessory proteins, *ii*) None of these synthases required a primer for initiation of synthesis, at least *in vitro,* and *iii*) An active XyG synthase complex made of *At*CslC4 and *At*XXT1 can be reconstituted *in vitro* and is sufficient for synthesizing β-glucan chains branched with up to three xylose (Xyl) side chains, *i.e*., XXXG subunit (for single-letter nomenclature of XyG see Tuomivaara, et al., 2015). These results provide new insights into the biochemical mechanism of plant cell wall β-glycan biosynthesis and *i*-GT-ray screening platform

represents a simple and powerful functional genomics tool for screening of processive synthase activities and can be adapted to other enzymes.

2. Materials and methods

2.1. Chemicals and Biological Materials

Manganese (II) chloride, magnesium chloride, potassium chloride, sodium bicarbonate from Sigma-Aldrich (St. Louis, MO, USA). HPLC-grade, Tris, HEPES, acetic acid, potassium phosphate buffers (pH 7), formic acid, scintillation liquid, Immobilon membranes, and SuperSignal West Femto Maximum Sensitivity Substrate, TMB substance, pCR™8/GW/TOPO™ TA Cloning Kit, Gateway LR Clonase II enzyme mix kit, PureLink RNA Mini Kit, streptavidin, Biotin, and ScintiVerse™ BD Cocktail were all from Fisher Scientific (Waltham, MA, USA). Glutathione S-Transferase (GST) was from GenScript (Piscataway, NJ, USA). Secondary antibody for anti-GST (mouse anti-goat IgG-HRP conjugate) was from Santa Cruz Biotechnology (Dallas, TX, USA). GST-Halo fusion protein, anti-Halo antibody, secondary antibody for anti-Halo (anti-Rabbit IgG HRP conjugate), GDP/UDP-GLO glycosyltransferase assay and TNT® Coupled Transcription/Translation system were from Promega (Madison, WI, United States). 96-well microplates and anti-GST antibody were from GE Healthcare Life Sciences (Pittsburgh, PA, USA). Uridine-diphosphate (UDP)-[^{14}C]glucose (9.25 GBq/mmol) were from PerkinElmer Life Sciences (Boston, MA, USA). UDP-xylose was purchased from CarboSource (Athens, GE, USA). UDP-glucose was from Sigma-Aldrich (St. Louis, MO, USA). 1-Step Human Coupled IVT Kit, Zeba™ Spin Desalting Column from Thermo scientific (Rockford, IL, USA). Lichenase β-(1,3;1,4)-D-4-glucanohydrolase (EC 3.2.1.73, from Bacillus sp) endo-β(1,4)-glucanase (cellulase from Trichoderma sp), and endo-β-mannanase (from *Aspergillus niger*) were purchased from Megazyme (Chicago, IL, USA). NucleoBond Xtra Midi kit was purchased from Machere-Nagel (Bethlehem, PA, USA). pANT7-cGST and pJFT7-nHalo vectors containing C-terminal GST or N-terminal Halo tags, respectively, were obtained from DNASU Plasmid Repository (Tempe, AZ, USA). pCR8/GW/TOPO-TA cloning and Gateway LR Clonase II enzyme mix kits were from Invitrogen (Carlsbad, CA, USA).

2.2. Cloning of Tagged GTs

Full-length protein coding sequences (CDS) clones of GTs were obtained from ABRC DNA Stock Center (Columbus, OH, United State). The CDS were amplified using the gene specific primer (**supplementary Table S5**) to create two forms of CDS, namely CDS with stop codon, and CDS without stop codon. All the CDS sequences were cloned into *pCR8/GW/TOPO-TA* vector, as an entry vector. The correct sequence and correctly oriented CDS in entry vector (150ng) were gateway cloned to expression vectors (150ng; *pANT7-cGST* and *pJFT7-nHalo*) using the Gateway LR Clonase II enzyme mix (2µL) kit in 8µL-volume reactions according to the manufacturer's instructions. Two forms of tagged GTs were generated: CDSs without stop codon were cloned to *pANT7-cGST* vector to create C-terminal GST tagged GTs fusion protein and CDSs with stop codon were cloned to *pJFT7-nHalo* vector to create N-terminal Halo tagged GTs fusion protein. The products of LR reactions were introduced into *E. coli* DH5α competent cells for plasmid extraction and purification. Plasmids were purified from bacteria cell cultures (200mL) using the NucleoBond Xtra Midi kit from Machere-Nagel according to the manufacturer's instructions. The purified plasmids are used directly for protein production using cell free *in vitro* coupled Transcription/Translation (IVTT) systems.

2.3. Plasmid DNA biotinylation

The plasmid DNA was linearized as follow: ~60µg of purified plasmid DNA was linearized with a restriction enzyme *Pfol*. (Thermo Fisher) according to manufacturer's recommendations and the digested plasmids were freeze-dried and resuspended in 10µL water and used for DNA biotinylation. Biotinylation was performed in Eppendorf tubes containing 1.25mg of EDC linker (1-ethyl-3-[3-dimethylaminopropyl] carbodiimide hydrochloride), to which 45µg of linearized plasmid (in 7.5µL) was added and immediately followed by addition of 5µL of 2.5 mM biotin hydrazide/imidazole solution. The mixture was vortexed and 20µL of 100mM imidazole pH 6 was added to mixture and incubated overnight at 37^0C. Unreacted EDC linker and imidazole were removed by spin desalting column (Zeba™ Spin Desalting Column) using 10mM PBS pH 7.2 containing 0.15M NaCl and 10mM EDTA. The biotinylated DNA (100-500ng/µL) was stored at -20^0C until use.

2.4. In vitro production of fusion Proteins

Fusion proteins were produced in tubes or directly on microplates as described in Bhattarai et al., (2024) and Javaid, et al., (2024). Microplates were coated with streptavidin (2-3µg) for overnight at 4^0C. After washing with PBS (3 times, 10min each) to remove excess of streptavidin, capture antibody (1:200 dilution) was then applied to the microwells (4h at 4^0C). Excess capture antibody was removed by washing with 10mM PBS (3 times, 10min each) and then microwells were blocked for 2-4h with 5%(w/v) fat-free dry milk in 10mM PBS at 4^0C. The microwells were washed with 10mM PBST (3 times, 10min each) before adding 1µg of biotinylated plasmid DNA dissolved in 50µL 5%(w/v) fat-free dry milk in 10 mM PBS) and allowed DNA binding to streptavidin for overnight at 4^0C. Unbound plasmid DNA was removed with 3 washes (100µL, 10min each) of 10mM PBS at room temperature. The microplates were used directly to generate GT-arrays by streamlining protein synthesis and binding as described above.

2.5. Immunoblotting Analysis

To determine the efficiency of protein production in the IVTT systems, 4 µL of expression reaction were separated on SDS-polyacrylamide gels (SDS-PAGE) and then transferred onto Immobilon membranes (Fisher Scientific) using the mini-protean tetra cell system (Bio-Rad). After transfer, the membranes were blocked for 1 h with 5%(w/v) fat-free dry milk in 10 mM phosphate buffer (PBS) containing 137 mM NaCl, 2.7 mM KCl pH 7.2. The membranes were incubated for 1 h with the primary antibody (anti-GST or anti-Halo) at 1:10,000 dilution in PBS, pH 7.2 containing 5%(w/v) fat-free milk and 0.05% (v/v) Tween-20. Excess of primary antibody was washed with PBS containing 0.05% (v/v) Tween-20 (four times, 15 min each) before incubation for 1 h with the secondary antibody conjugated to horse radish peroxidase (HRP) at 1:20,000 dilution in PBS, pH 7.2 containing 5%(w/v) fat-free milk and 0.05% (v/v) Tween-20. Excess of secondary antibody was removed by several washes (5-8 times, 15min each) of the membranes with PBS containing 0.05%(v/v) Tween-20. Detection of tagged proteins on the membranes was performed using SuperSignal West Femto Maximum Sensitivity Substrate and exposure to X-ray film (Research Products International Corp.).

2.6. Detect of complex formation

The Halo-*At*CslC4/*At*XXT1-GST and *At*CslC4-GST/Halo-*At*XXT1 combinations were produced through co-expression *in vitro* using cell-free IVTT system and their respective plasmid

DNA in tubes. The complexes produced were then applied to microwells were already pre-coated with appropriate capture antibodies (either anti-GST or anti-Halo). The GT arrays were prepared as described in Bhattarai et al., (2024) and Javaid, et al., (2024). After washing with 10mM PBS containing 0.05% (v/v) Tween-20 three times to remove unbound complexes, the immobilized complexes were detected as follows: when Halo-*At*CslC4/*At*XXT1-GST complex was immobilized *via* anti-GST capture antibody, the primary antibody used is anti-Halo (at 1/200 dilution, 50µL), which will recognize Halo-*At*CslC4. After washing of unbound anti-Halo antibody with 10 mM PBS containing 0.05% (v/v) Tween-20 (3 times, 10min, at room temperature), the secondary antibody goat anti-rabbit IgG fused to Horseradish peroxidase (HRP-anti-rabbit IgG, 1/400 dilution, 50µL) was applied. Excess HRP-anti-rabbit IgG was removed by washing with 10 mM PBS containing 0.05% (v/v) Tween-20 (3 times, 10min, at room temperature). The binding of HRP-anti-rabbit IgG to anti-Halo antibody was monitored using 1-Step Ultra TMB-ELISA solution (50µL/microwell). After 5-10min incubation, 50µL of 2M sulfuric acid were added to stop reaction before reading absorbance at 450nm using Biotek Synergy/HTX multi-mode reader (Winooski, VT, USA).

2.7. Transferase activity using radioactive Assays in a tube.

Radioactive assays (50 µL reaction) were performed in Eppendorf tubes according to published work (See **supplemental Table S1**) using the appropriate UDP-[^{14}C]sugars and 3-18 µL of expression protein reaction (protein concentration ~25 ng/µL, according to western blotting analysis). Reactions were carried out for 3h at 28^{0}C and stopped by adding 1mL of cold 70% ethanol for precipitation overnight at -20^{0}C. The pellets were washed (five times) with 1mL of cold 70% ethanol to remove excess of unused UDP-[^{14}C]Glc. The pellets were resuspended in 0.3 mL water and reprecipitated a second time by adding 1 mL of cold 70% ethanol to remove any remaining UDP-[^{14}C]Glc. The dried pellets were then resuspended in 0.3 mL water and the incorporation of radioactivity was measured (as cpm) using a LS 6500 multi-purpose scintillation counter (Beckman) after resuspension of the in 3-5 mL of liquid scintillation solution (Fisher Scientific).

2.8. XyG synthase and XyG glucan synthase assays on microplates (non-radioactive assays)

Standard XyG synthase assays were performed in 50 µL reaction volume containing UDP-Glc and UDP-Xyl (1 mM each) according to published work (see **supplemental Table S1**) on microplates. For XyG glucan synthase (XyG-GS) assays only UDP-Glc was used. The enzyme reactions were carried out for 3 h at 28^0C and the activity was measured using UDP GLO glycosyltransferase assay kit (Promega) according to manufacturer's protocol. Then the relative luminescence (RLU) signal was measured using Biotek Synergy/HTX multi-mode reader (Winooski, VT, USA). All assays were performed in duplicate or triplicate.

2.9. Desalting paper spray-mass spectrometry (DPS-MS) analysis

A high-resolution Q Exactive Orbitrap mass spectrometer (Thermo Scientific, San Jose, CA, USA) was used throughout this study. The commercial ESI ion source was removed to accommodate DPS. Data analysis was acquired by Thermo Xcalibur (3.0.63). The filter paper was cut into triangles (10 × 5 mm, height × base) after sequential sonication-assisted cleaning in acetone, methanol, and methanol/water (50/50 v/v, 15 min each). As reported previously in Wang, et al., (2020), for DPS-MS analysis, a 10 µL sample solution was dropped onto the paper triangle that was placed on top of a Kimwipe to facilitate the absorption by capillarity. Desalting was achieved by loading 10 µL of ACN/H_2O solution (90/10 v/v) onto the paper placed on top of another Kimwipe to wick the eluent containing salts and other chemicals. The paper triangle was then held in front of the MS inlet (8 mm away) using a high-voltage cable alligator clip, and 10 µL of ACN/H_2O/FA solution (10/90/1 v/v/v) was added directly onto the paper triangle to elute the target compounds for ionization upon application of a high voltage (3.5 kV) to the wetted paper.

2.10. Enzyme digestion of [^{14}C]products

The [^{14}C]products generated were split into five fractions for treatment with three individual hydrolases (lichenase, cellulase, mannanase) or buffer. Denatured proteins were used as negative control. Lichenase, mannanase, and cellulase treatments were carried out according to manufacturer's recommendation (Megazyme) by incubating [^{14}C]products with 1 unite of lichenase β-(1,3;1,4)-D-4-glucanohydrolase or endo-β(1,4)-glucanase (cellulase) or endo-β-mannanase in 500 µL reactions. Reactions were then stopped by boiling for 10 min and then 1 mL cold 70% ethanol was added to precipitate undigested [^{14}C]products, which is collected by

centrifugation at 15,000x*g* for 15 min, at 4^0C. Radioactivity retained in the pellets was measured (as cpm) using a scintillation counter as described above.

3. Results

3.1. Tagged glycan synthases produced through cell-free coupled IVTT are active in the absence of detergent, membrane lipids, or accessory proteins.

The *i*-GT-ray platform was originally developed and optimized using non-processive GTs such as *At*XXT1, *At*MUR2, *At*GUX1, and *At*FUT1 (Bhattarai et al., 2024). Processive GTs (synthases) were not tested on *i*-GT-ray platform. Here, we wanted to determine whether glycan synthases can also be produced in a soluble and active form. Because β-glycan synthases are inserted in the membranes via multi-transmembrane domains (TMDs, compared to a single TMD for most eukaryotic non-processive GTs), they are more difficult to produce *in vitro* as full-length and in a soluble active form. Here, we demonstrate that these processive GTs can be produced in an active form using cell-free coupled IVTT systems. N-terminal Halo-tagged and C-terminal GST-tagged versions of five synthases were generated and tested, namely, a cellulose synthase (*At*CesA4), two MLG synthases (*Hv*CslF6, and *Hv*CslH1), a glucomannan synthase (*At*CslA9), and a XyG-GS (*At*CslC4). Furthermore, we compared the efficiency of two cell-free coupled IVTT expression systems (TNT® Quick System and 1-Step Human Coupled IVT Kit) in producing these synthases. Before testing these GTs on *i*-GT-ray platform, we monitored the transferase activities of the fusion proteins in test tubes using radioactive assays and increasing volume (*i.e.*, 3, 6, 12, and 18μL) of cell-free coupled IVTT reactions. Our data show a clear positive correlation between transferase activities and the amount of produced fusion proteins used in the assays for the GTs tested (**Figure 1A**). Interestingly, while 1-Step Human Coupled IVT Kit produced active tagged GTs, TNT system did not seem to produce active enzymes (except for *At*CslA9, glucomannan synthase). Importantly, the position of the tag did not seem to affect transferase activities for these synthases. Western blotting analysis of some tagged GTs was performed to verify that fusion proteins were produced by the two expression systems (**supplemental Figure S1**). While 1-Step Human Coupled IVT system produced fusion proteins for all synthases at the expected size and with similar efficiency, TNT® Quick expression system produced more truncated forms, except for *At*CesA9 (**supplemental Figure S1**).

Next, we analyzed the [^{14}C]products generated by Halo-tagged version of these synthases through digestion with three specific hydrolases: Lichenase, mannanase, and cellulase. The fact that [^{14}C]products generated by these synthases were insoluble in 70% ethanol, suggests that they are of a degree of polymerization (DP) higher than 9-10. Radioactive products from *At*CslA4, and

*At*CesC4 were all digestible by cellulase, which solubilized 65-87% of the radioactivity, but not by lichenase and to some extent by mannanase (**Figure 1B**). On the other hand, when [^{14}C]products from *Hv*CslF6 and *Hv*CslH1 were treated with lichenase, the treatment resulted in solubilization of 75-85% of the radioactivity, while cellulase and mannanase solubilized only 15-35% and 2-30% of the radioactivity, respectively (**Figure 1B**). Two [^{14}C]products were generated by *At*CslA9, one from incubation with GDP-[^{14}C]Man alone, and the other from incubation with GDP-[^{14}C]Man and GDP-Glc. As expected, the presence of GDP-Glc enhanced the incorporation of [^{14}C]Man into ethanol-insoluble [^{14}C]products, and both [^{14}C]products were completely digested by mannanase (solubilization of 95-97% of radioactivity) (**Figure 1B**). Interestingly, the [^{14}C]products generated from GDP-[^{14}C]Man and GDP-Glc was more sensitive to cellulase (solubilization of ~70% of [^{14}C]products), which may suggest that the polymer produced has a higher ratio Glc to Man (**Figure 1B**).

Shorter oligosaccharides are also produced (DP less than 9). The presence of these shorter oligosaccharides allowed the detection of synthase activity and its products directly on *i*-GTray platform. We could streamline into a single workflow protein synthesis, immobilization, enzyme assay, and product detection by desalting paper spray-mass spectrometry (DPS-MS) (Wang, et al., 2020; Chiu, et al., 2021; Tanim-Al-Hassan, et al., 2024) of oligosaccharides produced by *At*CesA9 (**Figure 2B**), *At*CslC4 (**Figure 2C**), and *Hv*CeslF6 (**Figure 2D**). A series of oligosaccharides containing 4-9 glucose (G) residues (*m/z* 689, 851, 1013, 1175, 1337, and 1499) were detected in glucan synthase reactions catalyzed by Halo-*Hv*CslF6 and Halo-*At*CslC4 in presence of UDP-Glc (**Figure 2C** and **2D**). However, only two oligosaccharides containing three and four hexoses, Hex3 (*m/z* 527) and Hex4 (*m/z* 689), respectively, were detected from glucomannan synthase reaction catalyzed by *At*CslA9 in presence of GDP-Glc and GDP-Man (**Figure 2B**). All these oligosaccharides were absent in controls lacking donor substrates (*i.e.*, UDP-Glc, GDP-Glc and/or GDP-Man) (**Figure 2**). Furthermore, DPS-MS detected these ions with high accuracy (<3ppm, **supplemental Table S2**). Taken together, we concluded that *i*-GT-ray platform can be used broadly to couple synthesis, purification, and testing of both processive and non-processive GTs in a high-throughput manner, and DPS-MS is sensitive enough to detect their products.

3.2. AtCslC4 and AtXXT1 interact directly in vitro.

Many plant CW polysaccharides are synthesized by GTs that work as multi-protein complexes. Here, we sought to test whether *i*-GT-ray can be used to monitor enzyme activity of a multi-GT complex. We choose to test XyG synthase activity using *At*CslC4 and *At*XXT1 because bimolecular fluorescence complementation (BiFC) and *in vitro* pull-down assays showed that these two GTs colocalized in proximity (Chou, et al., 2012). However, whether these two GTs interact directly is not known. Therefore, we sought to test the interaction between *At*CslC4 (a XyG-GS) and *At*XXT1 (as described in Javiad et al., 2024) and the ability of the complex to produce xylosylated β-glucan oligosaccharides in presence of UDP-Glc and UDP-Xyl.

To ensure the *At*CslC4/*At*XXT1 complex is the result of a genuine PPI, two combinations *Halo-AtCslC4*/*AtXXT1-GST* and *AtCslC4-GST*/*Halo-AtXXT1* were co-expressed separately (in a tube) and the complexes were immobilized on microplates *via* either anti-Halo or anti-GST antibody (four ways of immobilization termed I, II, III, and IV, as depicted in **Figure 3A**). As indicated in **Figure 3B**, *At*CslC4 and *At*XXT1 clearly interacted directly with each other to form a complex *in vitro* regardless the position and nature of the tag. However, the efficiency of capturing the complexes ranged between 45% and 84% of the positive control (considered 100% binding) and was tag position dependent. The Halo-*At*CslC4/*At*XXT1-GST complex had the best immobilization rate on microplate coated with anti-GST antibody, *i.e*., 84% of the positive control.

3.3. AtCslC4/AtXXT1 complex is sufficient to generate xylosylated oligosaccharides in vitro.

When the captured complexes on microplate were incubated in the presence of UDP-Glc alone or UDP-Glc and UDP-Xyl, substantial activity was detected (*via* GLO^{TM} system) for all immobilized complexes (**Figure 3C**). The complexes that were immobilized through anti-GST capture antibody (*i.e*., designated I and III in **Figure 3C** corresponding to Halo-*At*CslC4/*At*XXT1-GST and Halo-*At*XXT1/*At*CslC4-GST, respectively) gave the best results with a slight enhancement of the activity in presence of both UDP-Glc and UDP-Xyl compared to UDP-Glc alone (**Figure 3C**).

DPS-MS detection of the products generated by Halo-*At*CslC4/*At*XXT1-GST and *At*CslC4-GST/Halo-*At*XXT1 complexes showed a series of oligosaccharides containing 5-9 glucose (G) residues with up to three Xyl (X) residues, [G_n+X_{1-3}]. As indicated in **Figure 4**, DPS-MS detected 12 ions in Halo-*At*CslC4/*At*XXT1-GST reaction matching mono-xylosylatd, di-xylosylated, and tri-xylosylated oligosaccharides (**Figure 4A, B**, and **C**, respectively), namely, [G_5+X_1] at *m/z*

961.32 (mass error 0.06ppm), [G_5+X_2] at *m/z* 1093.36 (mass error 1.97 ppm), [G_5+X_3] at *m/z* 1247.38 (mass error 3.38 ppm), [G_6+X_1] at *m/z* 1123.37 (mass error 2.69 ppm), [G_6+X_2] at *m/z* 1255.42 (mass error 2.54 ppm), [G_6+X_3] at *m/z* 1409.44 (mass error 2.01 ppm), [G_7+X_1] at *m/z* 1285.43 (mass error 2.15 ppm) and its sodium adduct ion at *m/z* 1307.41 (mass error 0.79), [G_7+X_2] at *m/z* 1417.47 (mass error 1.35 ppm), [G_8+X_1] at *m/z* 1469.46 (mass error 1.35 ppm), and [G_9+X_2] at *m/z* 1741,57 (mass error 0.91 ppm). None of these ions were detected in reactions containing UDP-Glc alone (**Figure 4**). Similarly, *At*CslC4-GST/Halo-*At*XXT1 complex produced 10 xylosylated oligosaccharides (**Figure 5**, **supplemental Table S3**). In addition to xylosylated oligosaccharides, both complexes did generate several cello-oligosaccharides containing 5-15 glucose, [$G_{5\text{-}15}$], that were detected by DPS-MS (**Figure 4D** and **supplemental Table S4**). It is important to mention that xylosylated cello-oligosaccharides were much less abundant in the reactions compared to cello-oligosaccharides (**Figure 4D**) and cannot be observed without zooming in spectra (**supplemental Figure S2**).

4. Discussion

Glycosyltransferases (GTs) play a central role in life. They catalyze the synthesis of structural and food storage polysaccharides, as well as metabolic small molecules, glycolipids, glycopeptides, and lipopolysaccharides. Previously we developed a screening platform (called *i*-GT-ray) for transferase activities that was used to screen non-processive GTs from family GT37 (Bhattarai et al., 2024). However, this platform was not tested for processive GTs for plant cell walls such as cellulose synthase, MLG synthase, glucomannan synthase, and XyG synthase. Here we present results showing that *i*-GTray platform is also appropriate for screening of processive GTs for plant cell wall synthesis. These processive GTs could be produced as tagged versions using cell-free IVTT systems in an active form in the absence of detergent, membrane lipids, or any accessory protein. We were somewhat surprised that all processive GTs tested on *i*-GTray platform were active, even the ones that could not be tested *in vitro* using traditional heterologous systems. For example, expressing *At*CslC4 or its homolog from nasturtium (*Tm*CslC) in *Drosophila* Schneider 2 or *P. pastoris* cells was not successful, as no activity was detected in extracts from the transgenic cells (Cocuron, et al., 2007).

Furthermore, the used of *i*-GT-ray allowed several new insights about these β-glycan synthase activities. The first insight was that none of the β-glycan synthase activities tested here required a primer for initiation of polymer synthesis *in vitro*. Assessing primer requirements using heterologous expression systems is challenging because there is always a possibility that small chains of β-glycan may co-purify with GTs. Morgan et al. (2013) showed that purified cellulose synthases already have small chains of cellulose in their translocation channels. For cellulose synthesis, there are contradicting reports about the mechanism of cellulose synthesis initiation. For example, compelling evidence that sitosterol-β-glucoside acts as a primer to initiate cellulose synthesis in plant was provided by Peng et al. (2002). However, a recent report demonstrates that cellulose synthesis initiation is primer-independent for two bacterial cellulose synthases (*Gluconacetobacter hansenii* and *Rhodobacter sphaeroides*) (McManus, et al., 2018). In *i*-GT-ray platform, not only processive GTs are produced *in vitro* in the absence of any oligosaccharides, but also the IVTT systems don't contain any NDP-sugars, which eliminates the risk of synthesis of a primer by the produced enzymes. Thus, our results suggest that these β-glycan synthase activities may be primer-independent (at least in our platform). If this holds true for some synthases *in vivo*, it suggests that these synthases may have activity that hydrolyzes nucleotide-sugar to

release NDP. Some GTs are known to possess such nucleotide-sugar hydrolysis activity (Ciesla and Bobak, 1998; Zhang, et al.,2001; Chavaroche, et ak., 2011). Although we did not detect any oligosaccharides having NDP attached to them, more experimental work is needed to determine the exact steps of the initiation mechanism. With the availability of *i*-GT-ray, it would be possible to investigate this aspect in more efficient way, which may provide valuable clues to understand the regulatory mechanism involved in the synthesis of plant cell wall polymers. For instance, it would be possible to investigate whether the oligosaccharide at the reducing end (termed sequence 1) of dicots glucuronoxylan serves as a primer or terminator of xylan biosynthesis (Peña, et al., 2007).

The second insight from this work is that none of the GTs tested on *i*-GT-ray platform required detergent, membrane lipids, or any accessory protein for activity. For instance, *At*CesA4 did not require detergent or lipids for activity, which contrasts a recent report showing *in vitro* reconstitution of cellulose synthase activity in proteoliposomes containing *Populus tremula* x *tremuloides* CesA8 (*Ptt*CesA8) or *Physcomitrella patens* CesA8 (*Pp*CesA8) (Purushotham, et al., 2016; Cho, et al., 2017). *Ptt*CesA8 loses its catalytic activity upon solubilization with detergent from these proteoliposome vesicles, which prompted the authors to conclude that enzymatic activity of *Ptt*CesA8 requires an intact lipid bilayer. On the other hand, bacterial BcsA has been shown to maintain catalytic activity in various detergents (Omadjela, et al., 2013). The most likely explanation is that addition of GST or Halo tag is sufficient in producing GTs with the proper folding at low yield (via IVTT) and replaces the need for membrane lipids or detergent. It has been shown that addition of GFP fusion domain enhanced proper GT folding (Pedelacq, et al., 2006 Moremen, et a., 2018).

MLG is one of the major storage carbohydrates in cereal grains, which consists of unsubstituted chains of β-D-glucosyl residues linked by both (1,3) and (1,4) linkages with no consecutive β-(1,3) linkages. Most grasses have MLGs with a defined ratio of β-(1,4) to β-(1,3) linkages in the range of 2.2–2.6:1 (Fincher, et al., 2004; Li, et al., 2006). When testing *Hv*CslF6 and *Hv*CslH1 on *i*-GT-ray platform, both enzymes showed similar levels of activity, which is in contrast with data from heterologous expression of these two synthases in Arabidopsis or tobacco (Fincher, et al., 2004; Li, et al., 2006). In these studies, the amount of MLG measured by enzymic digestion was low for *Hv*CslH1 (0.05% w/w) compared to *Hv*CslF6 (1.6% w/w). Furthermore, in our study, both enzymes generated products that were susceptible to lichenase, an MLG-specific

glucanohydrolase. Although more experimental work would be needed to elucidate the structure of MLG produced on *i*-GT-ray, this platform offers an easy way to investigate several aspects of MLG synthesis such as the mechanisms that regulate β-(1,3)-linkages insertion during MLG synthesis.

The third insight from this work concerns XyG synthesis. Earlier work on XyG synthesis demonstrated that microsomal membrane preparations can produce XyG polymers with the proper substitution patterns, namely, built up of [G_4-X_3]-based repeat units (referred to as XXXG) (Gordon and Maclachlan, 1989). However, all attempts to solubilize XyG synthase activity with detergents have failed. Thus, the protein composition of a functional XyG synthase isolated from plant tissue has never been accomplished. When *At*CslC4 and *At*XXT1 were co-expressed in *P. pastoris*, in an attempt to reconstitute XyG synthase activity, the transgenic cells produced only β-(1,4)-glucan chains (with various length), and extracts from these transgenic cells showed no XyG GS activity nor XyG synthase activity *in vitro* (Cocuron, et al., 2007). Currently, there is no evidence that XyG-synthesizing GTs interact directly. Bimolecular fluorescence complementation and *in vitro* pull-down assays showed that these GTs colocalized in close proximity (Chou, et al., 2012). In *i*-GT-ray platform, not only we showed that *At*CslC4 and AtXXT1 interact directly to form a complex *in vitro*, but the reconstituted *At*CslC4/*At*XXT1 complex was active (**Figure 3**) and sufficient for the synthesis of mono-, di-, and tri-xylosylated cello-oligosaccharides at lower yield (**Figures 4** and **5**), as well as non-xylosylated β-(1,4)-glucan chains (DP5-15, **supplemental Table S3**). Thus, *At*XXT1 in complex with *At*CslC4, is sufficient for the addition of multiple contiguous Xyl residues to nascent β-(1,4)-glucan chains, which challenges the conclusion from a recent report based on the 3D crystal structure of *At*XXT1 (Culbertson, et al., 2018), in which *At*XXT1 dimer alone cannot produce xylosylation patterns found in native XyG (*i.e.*, $[XXXG]_n$) because of steric constraints imposed by the acceptor binding cleft. However, our finding is in agreement with the report by Zhong et al., (2021) showing that *At*XXT1, *At*XXT2, AtXXT4 and *Os*XXT1 (the *At*XXT1 ortholog in rice) individually are capable of sequentially adding Xyl onto three contiguous Glc residues of cellohexaose (C_6) to generate GXXXGG and GXXXXG products. Cavalier and Keegstra (2006) also reported that under certain conditions (*i.e.,* longer incubation time and/or higher substrate ratios) *At*XXT1 was able to incorporate up to three Xyl residues onto C_6 to generate tri-xylosylated cellohexaose (GXXXGG), which prompted the authors to postulated that, after adding the first Xyl to cellohexaose, *At*XXT1 continues to add Xyl residues to adjacent

glucosyl residues closer to the reducing end by adding the second and third Xyl residues to produce GXXGGG and GXXXGG, respectively. Based on the observation that Arabidopsis *xxt1/xxt2* double mutant did not have detectable XyG, while single mutants have only a slight decrease in XyG content (Cavalier, et al. 2008), it can be deduced that *At*CslC4 with either *At*XXT1 or *At*XXT2 would be sufficient to synthesize tri-xylosylated subunits (XXXG) in plants, which in agreement with our data.

One remaining unresolved question in XyG synthesis is the cooperative mechanism associated with it. In this mechanism, incorporation of [^{14}C]Glc into ethanol-insoluble materials generated by microsomal membranes requires the presence of UDP-Xyl (Gordon and Maclachlan, 1989; Hayashi, 1989; Faik, et al., 2002), which implies that XyG-GS activity is regulated/controlled by the interacting XXT(s). In our platform, the *At*CslC4/*At*XXT1 complex showed substantial XyG-GS activity regardless the presence of UDP-Xyl (**Figure 3C**), suggesting that interaction with *At*XXT1 alone is not sufficient in imposing the cooperative mechanism. It is possible that XyG synthase complex requires proteins other than XXTs or factors (such as membrane environment) for the proper cooperative mechanism. Ongoing work aims at the reconstitution of XyG synthases using various combinations of CslCs and XXTs to understand the importance of each GTs in XyG synthesis and substitution pattern.

In conclusion, not only *i*-GT-ray platform helped gaining new information about β-glycan synthases such as cellulose synthase, MLG synthase, glucomannan synthase, and XyG synthase activities, but it opens the way to perform deeper analysis of the biosynthetic mechanism in more efficient manner in a short time frame. We believe that i-GT-ray will be a transformative tool for recombinant enzyme screening, enabling rapid screening of activities and speeding up the progress in glycochemistry and glycobiology.

Figure Legends

Figure 1. Activity of C-terminal GST-tagged and N-terminal Halo-tagged versions of five synthases: *At*CesA4, *At*CslA9, *At*CslC4, *Hv*CslF6 and *Hv*CslH1. **A)** Activities were monitored via radioactive assays according to published protocols and using increasing amount of synthesized fusion proteins (~25ng/mL) produced through 1-Step Human Coupled IVT Kit (IVT) or TNT® Quick systems (TNT). The donor substrates are indicated between parentheses. **B)** Ethanol-insoluble [^{14}C]products generated by Halo-tagged synthases were treated with cellulase, mannanase, or lichenase. Boiled fusion proteins were used as controls (see Materials and Methods). All assays were performed in triplicates and values are the averages ±SD.

Figure 2. Detection of *At*CslA9, *At*CslC4, and *Hv*CslF6 synthase activities on *i*-GT-ray platform. **A**) Transferase activities of three tagged synthases were measured using GLO^{TM} system (expressed as luminescence unit, RLU). The NDP-sugars used as donors are indicated for each synthase. Control reactions were lacking the NDP-sugars. **B**) Detection of *At*CslA9 reaction products via DPS-MS. **C**) Detection of *At*CslC4 reaction products via DPS-MS. **D**) Detection of *Hv*CsF6 reaction products via DPS-MS. Reaction products were detected using 10 µL from transferase reactions performed in microwells. Zoom in spectra are shown as 10X and 50X. Asterix indicates the peaks are contaminants from the donor substrates (GDP-Man or GDP-Glc). Assays were performed in triplicates and values are the averages ± SD.

Figure 3. Protein-protein interaction between *At*CslC4 and *At*XXT1. **A)** Schematic presentation of complexes made of tagged *At*CslC4 and *At*XXT1 produced through co-expression in the cell-free IVTT system. **B)** Immobilization on microwells *via* capture antibody (anti-Halo or anti-GST). In negative control 1, primary antibody is lacking; negative control 2, complex is lacking; and negative control 3, both complex and primary antibody are lacking. Positive control contains secondary antibody against capture antibody immobilized on the microplate. **C)** Enzyme activity of the *At*CslC4/*At*XXT1 complexes in presence of UDP-Glc alone or UDP-Glc and UDP-Xyl. Negative control is lacking the complex. Halo-*At*CslC4 is used as positive control for glucan synthase activity. All assays were performed in triplicates and values are the averages ± SD.

Figure 4. DPS-MS detection of mono-xylosylated (**A**), di-xylosylated (**B**), and tri-xylosylated cello-oligosaccharides (**C**), produced by Halo-*At*CslC4/*At*XXT1-GST complex in microwells in presence of UDP-Glc and UDP-Xyl or UDP-Glc alone. **D**) Comparison of relative abundance of xylosylated [G_n-X_x] and non-xylosylated cello-oligosaccharides [G_n] produced in presence of UDP-Glc and UDP-Xyl. G and X stand for Glc and Xyl, respectively. The reactions were performed at least two times.

Figure 5. DPS-MS detection of xylosylated cello-oligosaccharides produced by *At*CslC4-GST/Halo-*At*XXT1 complex in microwells in presence of UDP-Glc and UDP-Xyl. The reactions were performed at least two times.

Supplementary Information

The following supplemental materials are available.

Supplemental Figure S1. Summary of DPS-MS detection of oligosaccharides from reactions catalyzed by AtCslC4/AtXXT1 complexes.

Supplemental Figure S2. Full DPS-MS spectrum of products generated by transferase activity of Halo-*At*CslC4/*At*XXT1-GST complex.

Supplemental Table S1. List of the five processive GTs used in this study.

Supplemental Table S2. Mass error values of DPS-MS detection

Supplemental Table S3. Spectra of [G_n] ions detected by DPS-MS

Supplemental Table S4. List of oligosaccharides generated by Halo-AtCslC4/AtXXT1-GST and AtCslC4-GST/Halo-AtXXT1complexes and detected by DPS-MS.

Supplemental Table S5. Sequences of primers

Supplemental Figure Legends

Supplemental Figure S1. Western blotting analysis the tagged GTs produced in cell-free *in vitro* Transcription/Translation (IVTT) systems. Each lane was loaded with 4μL of IVTT reaction (~25ng/μL). **A)** C-terminal GST-tagged GTs were produced via 1-Step Human Coupled IVT kit (Thermo scientific) and detected with anti-GST antibody. Purified GST protein was used as standard to estimate protein concentration in IVTT reactions. BSA was used as negative control. **B)** N-terminal Halo-tagged GTs produced *via* TNT® Coupled Transcription/Translation system (Promega) were detected using anti-Halo antibody. GST and Halo tagged fusion proteins were produced at similar levels and the expected sizes, namely, 80.29 kDa for *At*XXT1-GST; 104.43 kDa for *At*CslC4-GST; 110.05 kDa for *Hv*CslH1-GST; 87.83 kDa for *At*CslA9-GST; 110.53 kDa for Halo-*At*CslC4; 152.61 kDa for Halo-*At*CesA4; 116.15 kDa for Halo-*Hv*CslH1; 103.75 kDa for Halo-*At*MUR3 and 93.93 kDa for Halo-*At*CslA9.

Supplemental Figure S2. Full DPS-MS spectrum of products generated by transferase activity of Halo-*At*CslC4/*At*XXT1-GST complex. Halo-AtCslC4 and AtXXT1-GST were produced by co-expression in 1-Step Human Coupled IVT system (IVTT reaction). The formed complex was immobilized on microplate and used for enzyme assay in presence or absence of UDP-Glc and UDP-Xyl.

Supplemental Table S1. List of the five processive GTs used in this study.

Activity (GT name)	CAZy family	Donor substrate	Acceptor	Linkage	References
XyG-Glucan synthase (*At*CslC4)	2	UDP-Glc	Unknown	β-1,4	Cocuron, et al., 2007
Cellulose synthase 4 (*At*CesA4)	2	UDP-Glc	Unknown	α-1,4	Purushotham, et al., 2016
Barley MLG synthase (*Hv*CSLF6)	2	UDP-Glc	Unknown	β-1,4; β-1,3	Buckeridge et al., 1999 Purushotham, et al., 2022
Barley MLG synthase (*Hv*CslH1)	2	UDP-Glc	Unknown	β-1,4; β-1,3	Buckeridge et al., 1999
Glucomannan synthase (*At*CslA9)	2	GDP-Man; GDP-Glc	Unknown	β-1,4	Dhugga, et al., 2004; Liepman, et al.,2005

Supplemental Table S2. DPS-MS analysis of products on GT-array. Transferase activities tested were Halo-tagged versions of *Hv*CslF6, *At*CslC4, and *At*CslA9 (see Figure 2). Mass error values lower than 5ppm is an indication of detection accuracy. G, M, and Hex stand for Glc, Man, and hexose, respectively.

GT name	Acceptor/product	Detected ions (*m/z*)	Theoretical (*m/z*)	Mass error (ppm)
Halo-*Hv*CslF6	Tetrasaccharide (G4)	689.21295 $[G4+Na]^+$	689.21108	2.71
	Pentasaccharide (G5)	851.26471 $[G5+Na]^+$	851.26390	0.95
	Hexasaccharide (G6)	1013.31793 $[G6+Na]^+$	1013.31673	1.18
	Heptasaccharide (G7)	1175.37036 $[G7+Na]^+$	1175.36955	0.69
	Octasaccharide (G8)	1337.42383 $[G8+Na]^+$	1337.42237	1.09
	Nonasaccharide (G9)	1499.47321 $[G9+Na]^+$	1499.47520	1.33
Halo-*At*CslA9	Trisaccharide (Hex3)	527.15876 $[Hex3+Na]^+$	527.15826	0.95
	Tetrasccharide (Hex4)	689.21130 $[Hex4+Na]^+$	689.21108	0.32
Halo-*At*CslC4	Tetrasaccharide (G4)	689.21306 $[G4+Na]^+$	689.21108	2.87
	Pentasaccharide (G5)	851.26599 $[G5+Na]^+$	851.26390	2.46
	Hexasaccharide (G6)	1013.31806 $[G6+Na]^+$	1013.31573	2.30
	Heptasaccharide (G7)	1175.37233 $[G7+Na]^+$	1175.36955	2.37
	Octasaccharide (G8)	1337.42662 $[G8+Na]^+$	1337.42237	3.18
	Nonasaccharide (G9)	1499.47502 $[G9+Na]^+$	1499.47520	0.12

Supplemental Table S3: List of oligosaccharides detected by DPS-MS along with their spectra and mass error values. The oligosaccharides were generated by two complexes of *At*CslC4 and *At*XXT1, namely, Halo-*At*CslC4/*At*XXT1-GSTand *At*CslC4-GST/Halo-*At*XXT1. G stands for Glc. Tests were carried in duplicate.

Oligosaccharide	*At*CslC4-GST/Halo-*At*XXT1 DPS-MS spectra	Halo-*At*CslC4/*At*XXT1-GST DPS-MS spectra
$[G_5 +H]^+$ Theoretical *m/z* 829.28196	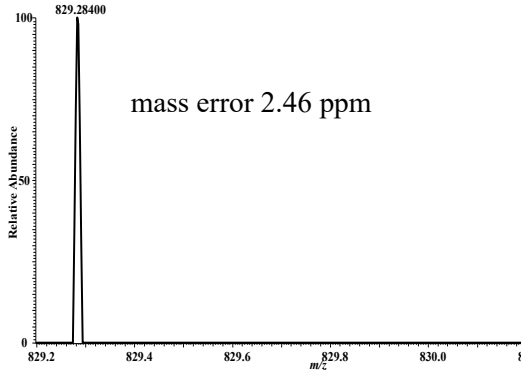	
$[G_5 +Na]^+$ Theoretical *m/z* 851.26390	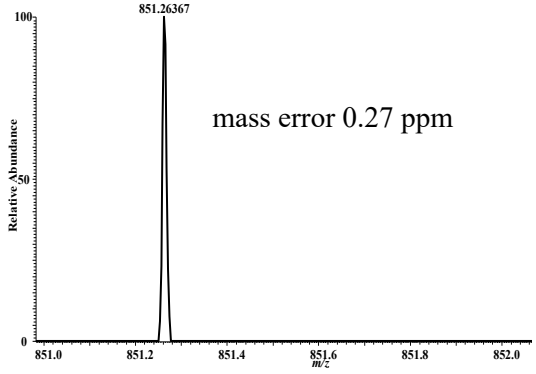	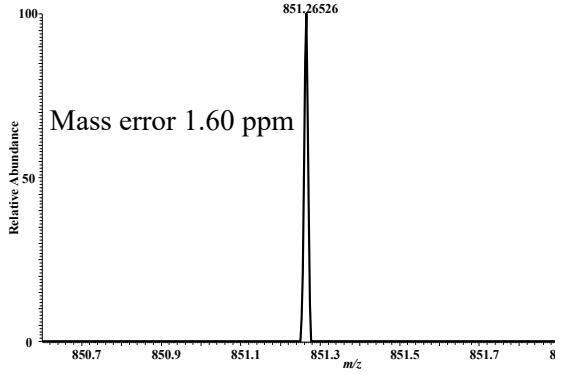
$[G_6 +H]^+$ Theoretical *m/z* 991.33478	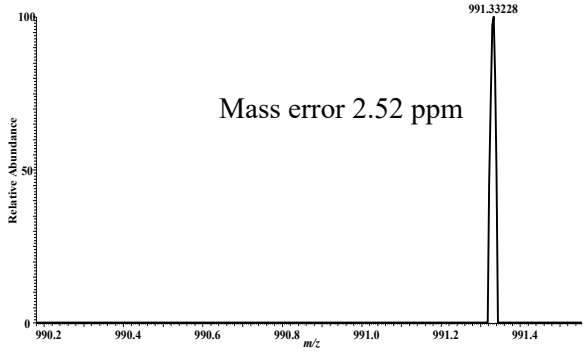	
$[G_6 +Na]^+$ Theoretical *m/z* 1013.31673	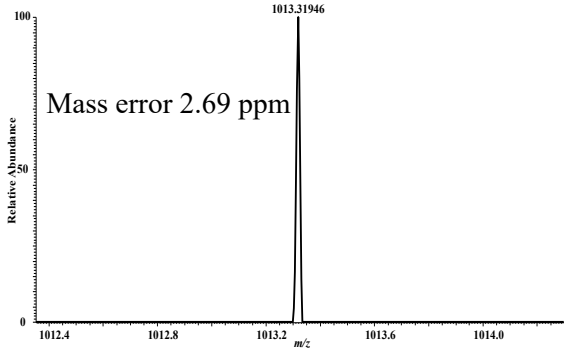	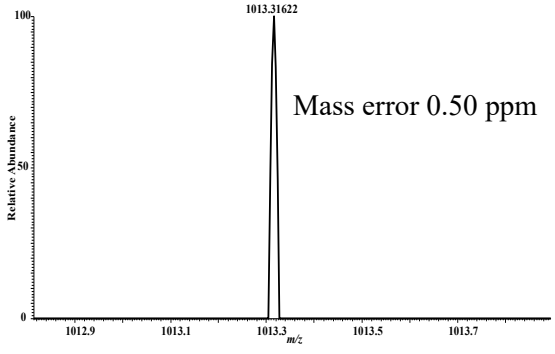

$[G_7 + H]^+$ Theoretical *m/z* 1153.38760	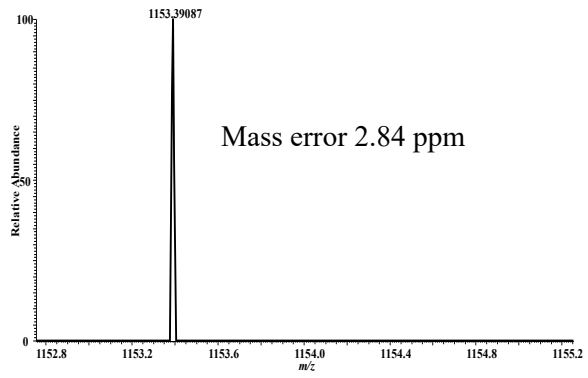	
$[G_7 + Na]^+$ Theoretical *m/z* 1175.36955	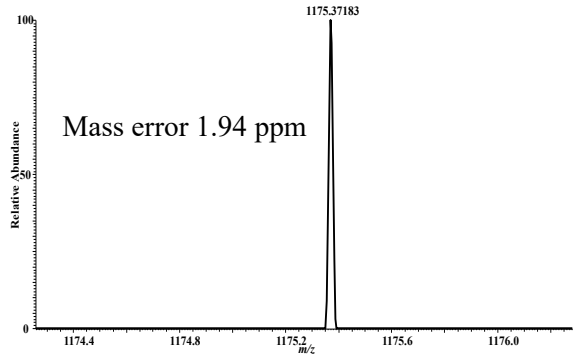	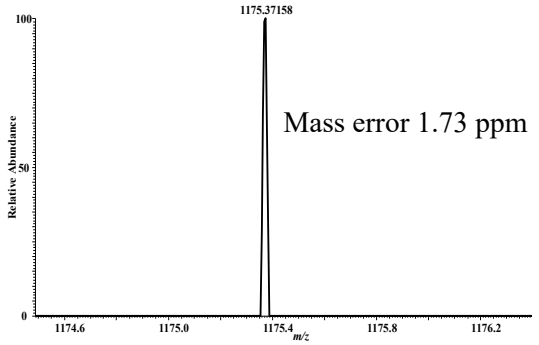
$[G_8 + Na]^+$ Theoretical *m/z* 1337.42237	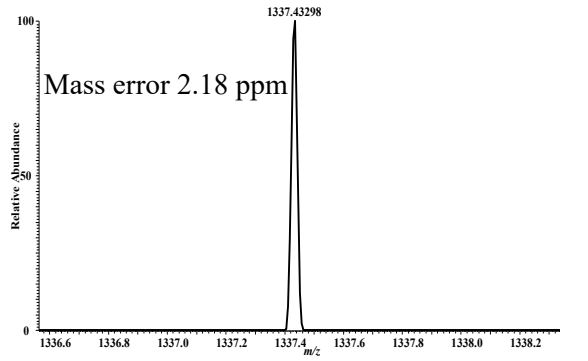	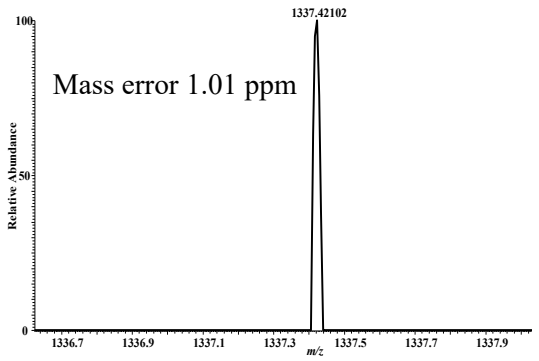
$[G_9 + Na]^+$ Theoretical *m/z* 1499.47520	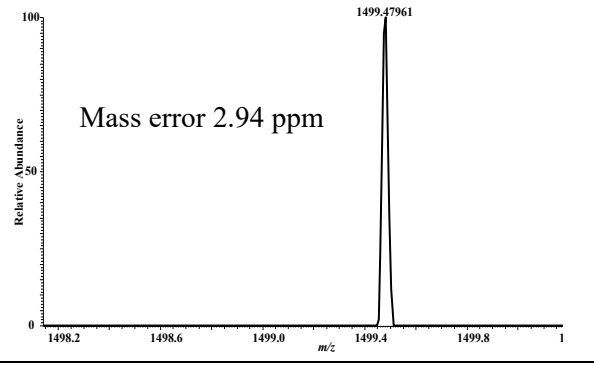	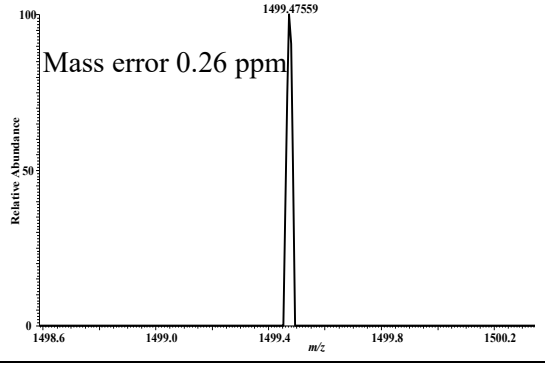

$[G_{10}+Na]^+$ Theoretical *m/z* 1661.52802	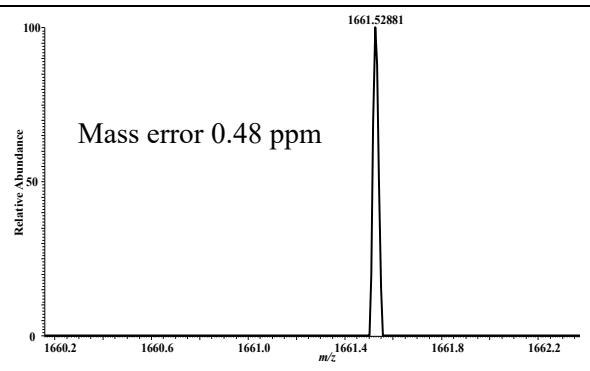	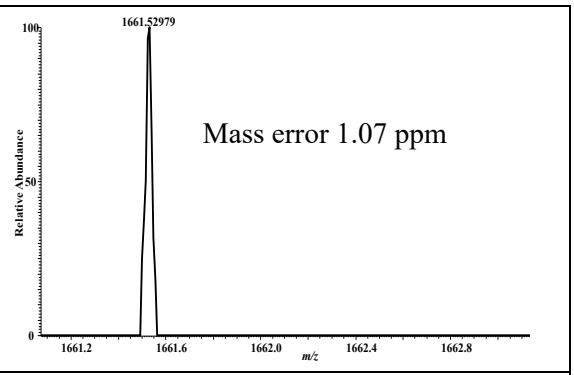
$[G_{11}+Na]^+$ Theoretical *m/z* 1823.58084	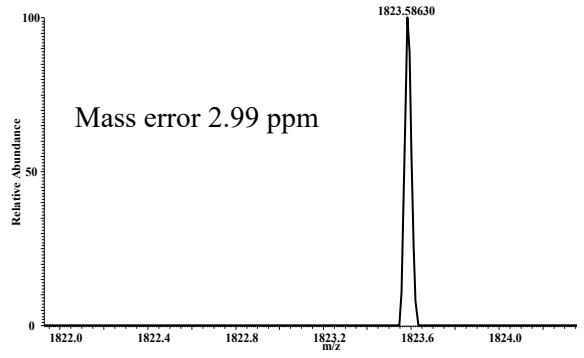	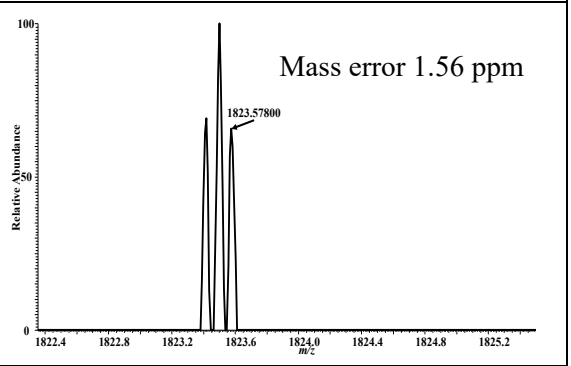
$[G_{12}+Na]^+$ Theoretical *m/z* 1985.63367	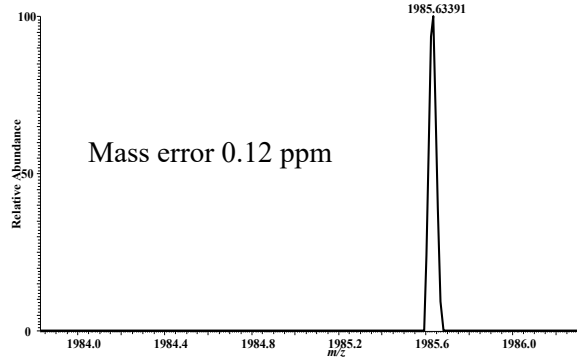	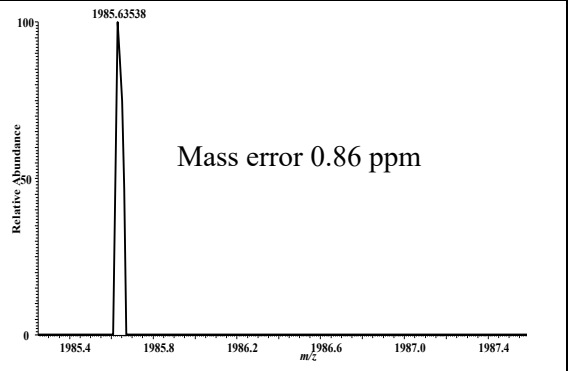
$[G_{13}+Na]^+$ Theoretical *m/z* 2147.68649	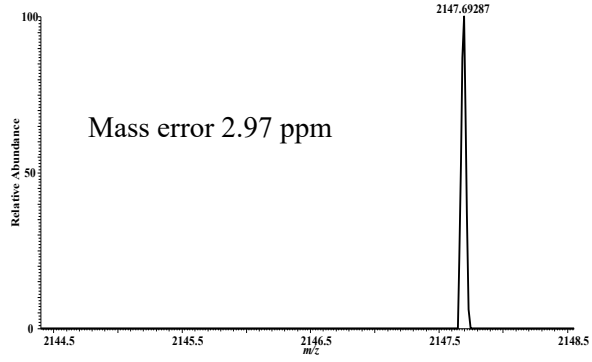	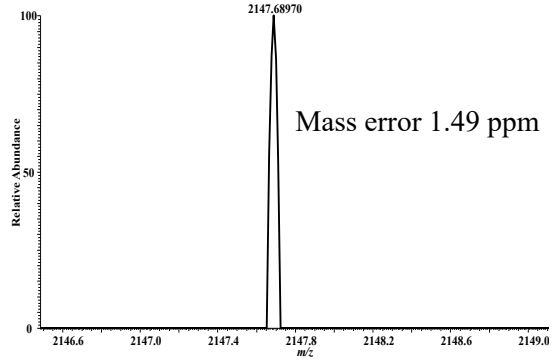

$[G_{14} + Na]^+$ Theoretical *m/z* 2309.73931	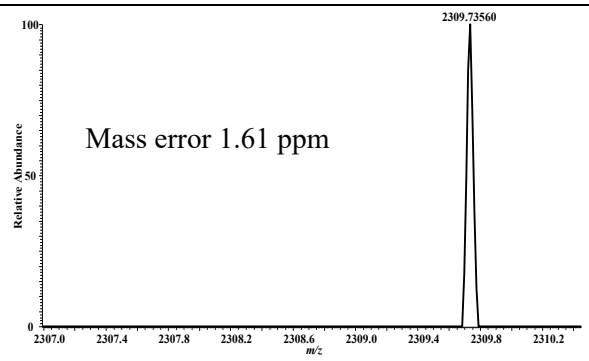	
$[G_{15} + Na]^+$ Theoretical *m/z* 2471.79214	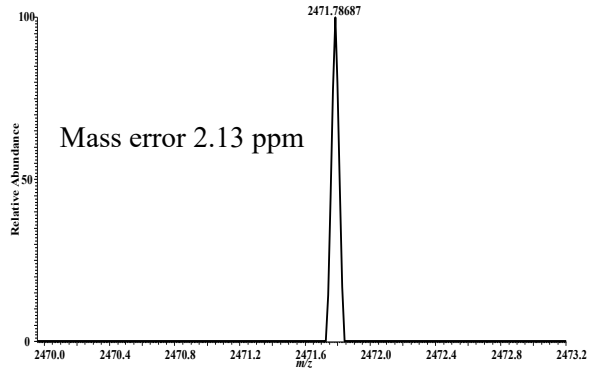	

Supplemental Table S4: List of oligosaccharides generated by Halo-*At*CslC4/*At*XXT1-GST and *At*CslC4-GST/Halo-*At*XXT1complexes and detected by DPS-MS. ($+H^+$) and (+Na) indicate protonated and sodiated ions, respectively. G and X stand for Glc and Xyl, respectively.

	Halo-*At*CslC4/*At*XXT1-GST complex			
n	[G_n+0X]	[G_n+1X]	[G_n+2X]	[G_n+3X]
5	829.28400(+H)	961.32416(+H)	1093.36853(+H)	
	851.26367(+Na)		1115.34839(+Na)	1247.38647(+Na)
6	991.33228(+H)	1123.37402(+H)	1255.42249(+H)	
	1013.31946(+Na)			1409.44067(+Na)
7	1153.39087(+H)	1285.43262(+H)	1417.47021(+H)	
	1175.37183(+Na)	1307.41284(+Na)		
8	1337.43298(Na)	1469.46265(+Na)		
9	1499.47961(+Na)		1741.57935(+H)	
10	1661.52881(+Na)			
11	1823.58630(+Na)			
12	1985.63391(+Na)			
13	2147.69287(+Na)			
14	2309.73560(+Na)			
15	2471.78687(+Na)			
	***At*CslC4-GST/Halo-*At*XXT1**			
n	[G_n+0X]	[G_n+1X]	[G_n+2X]	[G_n+3X]
5			1093.36584(+H)	
	851.26526(+Na)			1247.39343(+Na)
6	1013.31622(+Na)	1145.36169(+Na)	1277.40198(+Na)	
7		1285.42822(+H)		
	1175.37158(+Na)		1439.45776(+Na)	
8		1447.48450(+H)		1711.56604(+H)
	1337.42102(+Na)		1601.50964(+Na)	1733.55273(+Na)
9	1499.47559(+Na)			
10	1661.52979(+Na)			
11	1823.57800(+Na)			
12	1985.63538(+Na)			
13	2147.68970(+Na)			

Supplemental Table S5. Sequences of primers used for cloning into pCR8/GW/TOPO/TA vector before using the Gateway LR Clonase II enzyme to transfer the genes to expression vectors. Forward and reverse primers are listed as F or R, respectively.

Gene	Primer	Sequence
*At*CslC4	F	ATGGCTCCAAATTCAGTAGCAGTGAC
	R without stop	GCTGATCTGTTCTCCGATCAAATCCAAC
	R with stop	CTAGCTGATCTGTTCTCCGATCAAATCC
*At*CslA9	F	ATGGAGCTAGGAGATACGACGTCG
	R without stop	ATGGTTAGGCACAATTGTCCCAATTTGCC
	R with stop	TCAATGGTTAGGCACAATTGTCCCAATTTG
*At*CslA4	F	ATGGAACCAAACACCATGGCCAG
	R without stop	ACAGTCGACGCCACATTGCTTC
	R with stop	TTAACAGTCGACGCCACATTGCTT
*Hv*CslF6	F	ATGGCGCCAGCGGTGGCC
	R without stop	ATGGAGCCAGCCATAGAGCCCTGTGTC
	R with stop	TCAATGGAGCCAGCCATAGAGCCCTGTG
*Hv*CslH1	F	ATGGCGGGCGGCAAGAAGCTG
	R without stop	GTTCCTTGTGCAGAGGTGCACGAACGCA
	R with stop	TTAGTTCCTTGTGCAGAGGTGCACGAACGC

Acknowledgments

We thank Dr. Vel Murugan, Dr. Joshua LaBaer, and Jennifer Van Duine from Biodesign Institute at Arizona State University (Tempe, AZ) for their efforts to assist in early stages of this work. This work was funded primarily by the USDA (Award Number 2019-67030-29670) and Ohio University Research Committee (OURC).

Literature Cited

Amos, RA, Mohnen, D. (2019) Critical Review of Plant Cell Wall Matrix Polysaccharide Glycosyltransferase Activities Verified by Heterologous Protein Expression. Front. Plant Sci., **10**: 00915

Atmodjo, MA, Sakuragi, Y, Zhu, X, Burrell, AJ, Mohanty, SS, Atwood III, JA, Orlando, R, Scheller, HV, Mohnen, D (2011) Galacturonosyltransferase (GAUT)1 and GAUT7 are the core of a plant cell wall pectin biosynthetic homogalacturonan:galacturonosyltransferase complex. Proc. Natl. Acad. Sci. USA, **108**: 20225-20230

Bhattarai, M, Wang, Q, Javaid, T, Venkataraghavan, A, Al Hassan, MT, O'Neil, M, Tan, L, Chen, H, Faik A (20204) Streamlining assays of glycosyltransferases activity using *in vitro* GT-array (*i*-GT-ray) platform: Application to family GT37 fucosyltransferases. Journal of Biological Chemistry. (https://www.jbc.org/article/S0021-9258(24)00110-8/fulltext)

Buckeridge MS, Vergara CE, Carpita NC. (1999) The mechanism of synthesis of a mixed-linkage (1-->3), (1-->4)beta-D-glucan in maize. Evidence for multiple sites of glucosyl transfer in the synthase complex. Plant Physiol.; **120**:1105-16

Burton, RA, Wilson, SM, Hrmova, M, Harvey, AJ, Shirley, NJ, Medhurst, A, Stone, BA, Newbigin, EJ, Bacic, A, Fincher, GB (2006). Cellulose synthase-like CslF genes mediate the synthesis of cell Wall (1,3;1,4)-β-D-Glucans. Science **311**:1940–1942

Cavalier, DM., Keegstra, K. (2006) Two Xyloglucan Xylosyltransferases Catalyze the Addition of Multiple Xylosyl Residues to Cellohexaose. J. Biol. Chem., **281**:34197–34207

Cavalier DM, et al. (2008) Disrupting two Arabidopsis thaliana xylosyltransferase genes results in plants deficient in xyloglucan, a major primary cell wall component. Plant Cell **20**:1519–1537

Chavaroche, A. A. E.; van den Broek, L. A. M.; Springer, J.; Boeriu, C.; Eggink, G. (2011) Analysis of the polymerization initiation and activity of Pasteurella multocida heparosan synthase PmHS2, an enzyme with glycosyltransferase and UDP-sugar hydrolase activity. J. Biol. Chem., **286**: 1777−1785

Chiu, K-Y., Wang, Q., Gunawardena, H. P., Held, M., Faik, A., and Chen, H. (2021) Desalting paper spay mass spectrometry (DPS-MS) for rapid detection of glycans and glycoconjugates. *Int. J. Mass Spec*. **469**, 116688

Chou, Y-H, Pogorelko, G, Young, ZT, Olga A. Zabotina, OA (2015) Protein–Protein Interactions Among Xyloglucan-Synthesizing Enzymes and Formation of Golgi-Localized Multiprotein Complexes. Plant Cell Physiol., **56**: 255–267

Chou YH, Pogorelko G, Zabotina OA.(2012) Xyloglucan xylosyltransferases XXT1, XXT2, and XXT5 and the glucan synthase CSLC4 form Golgi-localized multiprotein complexes. Plant Physiol., **159**:1355-66

Cho, SH, Purushotham, P, Fang, C, Maranas, C, Diaz-Moreno, SM, Bulone, V, Zimmer, J, Kumar, M, Nixon, BT (2017). Synthesis and Self-Assembly of Cellulose Microfibrils from Reconstituted Cellulose Synthase. Plant Physiol., **175**: 146-156

Ciesla, W. P., Jr., and Bobak, D. A. (1998) *Clostridium difficile* Toxins A and B Are Cation-dependent UDP-glucose Hydrolases with Differing Catalytic Activities. J. Biol. Chem., **273**: 16021–16026

Cocuron, JC, Lerouxel, O, Drakakaki, G, Alonso, AP, Liepman, AH, Keegstra, K. Raikhel, N, Wilkerson, CG (2007) A gene from the cellulose synthase-like C family encodes a β-1,4 glucan synthase. Proc. Natl. Acad. Sci. USA, **104**:8550–8555

Culbertson, AT., Ehrlich, JJ., Choe, JY., Honzatko, RB., Zabotina, OA (2018) Structure of xyloglucan xylosyltransferase 1 reveals simple steric rules that define biological patterns of xyloglucan polymers. Proc. Natl. Acad. Sci. U.S.A., **115**: 6064-6069

Dhugga, K. S.; Barreiro, R.; Whitten, B.; Stecca, K.; Hazebroek, J.; Randhawa, G. S.; Dolan, M.; Kinney, A. J.; Tomes, D.; Nichols, S. (2004) Guar seed β-mannan synthase is a member of the cellulose synthase super gene family. *Science*, **303**: 363– 366

Dhugga, K. (2007) Maize biomass yield and composition for biofuels. Crop Sci., **47**:2211-2227

Doblin, MS, Pettolino, FA, Wilson, SM, Campbell, R, Burton, RA, Fincher, GB, Newbigin, E, Bacic, A (2009) A barley cellulose synthase-like CSLH gene mediates (1,3;1,4)-beta-D-glucan synthesis in transgenic Arabidopsis. Proc. Natl. Acad. Sci. U.S.A. **106**:5996-6001

Endler, A., Kesten, C., Schneider, R., Zhang, Y., Ivakov,A., Froehlich, A., Funke, N., Persson, S. (2015) A Mechanism for Sustained Cellulose Synthesis during Salt Stress. Cell **162**: 1353–1364

Faik, A. (2010) Xylan Biosynthesis: News from the Grass. Plant Physiol., **153**:396-402

Faik A., Price NJ , Raikhel NV , Keegstra K (2002) An Arabidopsis gene encoding an alpha-xylosyltransferase involved in xyloglucan biosynthesis. Proc Natl Acad Sci USA **99**:7797–7802

Ferguson, LR (1999) Wheat bran and cancer: The role of dietary fiber. Asia Pac. J. Clin Nutr., **8**:17-25

Fincher, G.B.; Stone, B.A. CEREALS|Chemistry of Nonstarch Polysaccharides. In Encyclopedia of Grain Science;Wrigley, C., Ed.; Elsevier: Amsterdam, The Netherlands, 2004; pp. 206–223

Gordon, R, Maclachlan, G (1989) Incorporation of UDP-[^{14}C]Glucose into xyloglucan by Pea membranes. Plant Physiol., **91**:373–378

Hayashi, T (1989) Xyloglucans in the Primary Cell Wall. Annu Rev Plant Physiol Plant Mol Biol., **40**:139–168

Javaid, T., Bhattarai, M., Venkataraghavan, A., Held, M., Faik, A. (2024) specific protein interactions between rice members of the GT43 and GT47 families form various central cores of putative xylan synthase complexes. Plant J., DOI: 10.1111/tpj.16640

Jiang, N., Wiemels, R.E., Soya, A., Whitley, R., Held, M., Faik, A. (2016) Composition, assembly, and trafficking of a wheat xylan synthase complex (XSC). Plant Physiol., **170**: 1999-2023. doi: 10.1104/pp.15.01777

Kim, S-J, Chandrasekar, B, Rea, AC, Danhof, L, Zemelis-Durfee, S, Thrower, N, Shepard, ZS, Pauly, M, Brandizzi, F, Keegstra, K (2020) The synthesis of xyloglucan, an abundant plant cell wall polysaccharide, requires CSLC function. Proc Natl Acad Sci USA, **117**: 20316-20324

Li, W., Cui, S.W. Kakuda, Y. (2006) Extraction, fractionation, structural and physical characterization of wheat β-D-glucans. Carbohydr. Polym., **63**: 408–416

Liepman, AH, Wilkerson, CG, and Kenneth Keegstra (2005) Expression of cellulose synthase-like (Csl) genes in insect cells reveals that CslA family members encode mannan synthases. Proc. Natl. Acad. Sci. USA, **102**:2221–2226

McManus, JB, Yang, H, Wilson, L, Kubicki, JD, Tien, M (2018) Initiation, Elongation, and Termination of Bacterial Cellulose Synthesis. ACS Omega, **3**: 2690−2698

Morgan, JLW., Strumillo, J., Zimmer, J. (2013) Crystallographic snapshot of cellulose synthesis and membrane translocation. Nature **493:** 181–186

Moremen, K.W., Ramiah, A., Stuart, M., Steel, J., Meng, L., Forouhar, F., Moniz, H.A., Gahlay, G., Gao, Z., Chapla, D., Wang, S., Yang, J.Y., Prabhakar, P.K., Johnson, R., Rosa, M.D., Geisler, C., Nairn, A.V., Seetharaman, J., Wu, S.C., Tong, L., Gilbert, H.J., LaBaer, J., Jarvis, D.L. (2018) Expression system for structural and functional studies of human glycosylation enzymes. Nat Chem Biol.; **14**:156-162

Omadjela O, et al. (2013) BcsA and BcsB form the catalytically active core of bacterial cellulose synthase sufficient for in vitro cellulose synthesis. Proc. Natl. Acad. Sci. USA, **110**:17856–17861

Pedelacq, J.D., Cabantous, S., Tran, T., Terwilliger, T.C., Waldo, G.S. (2006) Engineering and characterization of a superfolder green fluorescent protein. *Nat Biotechnol*.; **24**:79–88

Peña MJ, Zhong R, Zhou GK, Richardson EA, O'Neill MA, Darvill AG, York WS, Ye ZH (200) *Arabidopsis irregular xylem8* and *irregular xylem9*: Implications for the Complexity of Glucuronoxylan Biosynthesis Plant Cell, **19**:549–563

Peng, L.; Kawagoe, Y.; Hogan, P.; Delmer, D. (2002) Sitosterol-betaglucoside as primer for cellulose synthesis in plants. Science, **295**: 147−150

Purushotham, S. H. Cho, S. M. Díaz-Moreno, M. Kumar, B. T. Nixon, V. Bulone, J. Zimmer, A (2016) single heterologously expressed plant cellulose synthase isoform is sufficient for cellulose microfibril formation in vitro. *Proc. Natl. Acad. Sci. U.S.A.* **113**:11360–11365

Purushotham, P., Ho, R., Yu, L., Fincher, G.B., Bulone, V., Zimmer, J. (2022) Mechanism of mixed-linkage glucan biosynthesis by barley cellulose synthase-like CslF6 (1,3;1,4)-β-glucan synthase. Sci Adv.; **8**:eadd1596. doi: 10.1126/sciadv. add1596

Slabaugh, E, Davis, JK, Haigler, CH, Yingling, YG, Zimmer, J (2014) Cellulose synthases: new insights from crystallography and modeling. Trends Plant Sci 19:99–106

Tanim-Al-Hassan, Md., Chen, X., Fnu P.I.J., Francis J. Osonga, F.J., Sadik, O.A., Li, M., and Chen, H. (2024) Rapid Detection of Per- and Polyfluoroalkyl Substances (PFAS) Using Paper Spray-Based Mass Spectrometry. *Journal of Hazardous Materials*, **465**:133366

Taylor, NG., Howells, RM., Huttly, AK., Vickers, K., Simon R. Turner SR. (2003) Interactions among three distinct CesA proteins essential for cellulose synthesis. Proc. Natl. Acad. Sci. USA, **100**:1450-1455

Tuomivaara ST, Yaoi K, O'Neill MA, York WS. (2015) Generation and structural validation of a library of diverse xyloglucan-derived oligosaccharides, including an update on xyloglucan nomenclature. Carbohydrate Research*.,* **402**:56–66

Wang, Q, Bhattarai, M, Zhao, P, Alnsour, T, Held, M, Faik, A, Chen, H (2020) Fast and Sensitive Detection of Oligosaccharides Using Desalting Paper Spray Mass Spectrometry (DPS-MS). J. Am. Soc. Mass Spectrom, **31**: 2226-2235

Voiniciuc, C, Dama, M, Gawenda, N, Stritt, F, Pauly, M (2019) Mechanistic insights from plant heteromannan synthesis in yeast. Proc. Natl. Acad. Sci. USA, **116**:522–52

Welner, DH, Shin, D, Tomaleri, GP, DeGiovanni, AM, Tsai, AY-L, Tran, HM, et al. (2017) Plant cell wall glycosyltransferases: High-throughput recombinant expression screening and general requirements for these challenging enzymes. PLoS ONE **12**: e0177591

Zabotina OA, et al. (2008) Arabidopsis XXT5 gene encodes a putative alpha-1,6-xylosyltransferase that is involved in xyloglucan biosynthesis. Plant J **56**:101–115

Zhang, Y., Wang, P. G., and Brew, K. (2001) Specificity and Mechanism of Metal Ion Activation in UDP-galactose:β-Galactoside-α-1,3-galactosyltransferase. J. Biol. Chem. **276**: 11567–11574

Zhong, R, Phillips, DR, Zheng-Hua Ye, Z-H (2021) A Single Xyloglucan Xylosyltransferase Is Sufficient for Generation of the XXXG Xylosylation Pattern of Xyloglucan. Plant Cell Physiol. **62**:1589–1602

Zeng, W., Lampugnani E.R., Picard, K.L., Song, L., Wu, A-M., Farion, I. M., Zhao, J., Ford, K., Doblin, M.S., Bacic, A. (2016) Asparagus IRX9, IRX10, and IRX14A Are Components of an Active Xylan Backbone Synthase Complex that Forms in the Golgi Apparatus. Plant Physiol., **171**: 93-109

Highlights

Synthases are responsible for the synthesis of β-glycans of plant cell walls. However, several questions about their biochemical mechanisms remain without answers because of the lack of a method that would allow the production and purification of these enzymes *in vitro*. This report uses an *in vitro* GT-array (*i*-GTray) platform that streamlines *in vitro* protein synthesis, enzyme activity measurement, and product detection in a single workflow. Using this platform, we demonstrate that *i)* synthases can be produced in active form in the absence of detergent, membrane lipids, or accessory proteins, *ii)* synthases for cellulose, xyloglucan, (gluco)mannan, and β-(1,3)(1,4)-mixed-linkage glucan do not require primers to initiate synthesis process, and *iii)* active synthase complexes (such as *At*CslC4/*At*XXT1 complex) can be reconstituted through protein-protein interactions. *i*-GT-ray platform can be applied to enzymes other than glycosyltransferases and may help in the identification of novel enzymes important for crop improvement and food security in more efficient way.